

- was transfected into HeLa cells with Lipofectamine Plus (Gibco-BRL, Invitrogen). For transient expression experiments, cells were examined 20 to 24 hours after transfection. Stable expressing cells were obtained after approximately 2 weeks of selection in G418 (Gibco-BRL, Invitrogen) containing growth medium. Cx43-TC was also expressed in cardiac myocytes, NIH 3T3, and NRK cells, showing similar fluorescence patterns, trafficking, and functionality.
17. D. W. Laird *et al.*, *Microsc. Res. Tech.* **52**, 263 (2001).
 18. FLAsH-EDT₂ or ReAsH-EDT₂ was used at final concentrations of 1 and 2.5 μ M, respectively, in presence of EDT (10 μ M). The labeling was performed for one hour at 37°C in 1x Hank's Balanced Salt Solution (HBSS, Gibco-BRL, Invitrogen) supplemented with D⁺ glucose (1g/l). Free and nonspecifically bound ligands were removed by washing with EDT (250 μ M) (in HBSS+glucose). FLAsH-labeled cells were fixed with 4% formaldehyde (from paraformaldehyde), permeabilized, and stained with Cx43-specific monoclonal antibody (BD Biosciences, PharMingen, San Diego, CA).
 19. Junctional conductance was measured with the use of the dual whole-cell patch clamp. Briefly, each cell of a pair is voltage clamped independently with a separate patch clamp amplifier (Axopatch-200A, Axopatch-200B, Axon Instruments, Union City, CA). By stepping the voltage in one cell and keeping the other constant, junctional current I_j is observed directly as a change in current in the unstepped cell. Thus, for stepping cell 1, g_j is obtained by dividing the change in I_j by the change in V_1 . Currents were digitized using Digidata 1200B (Axon Instruments) and analyzed with pCLAMP8 software (Axon Instruments). Pairs of gap junctions were randomly selected for recording. The large variance in conductance is due to a large variability in plaque size (proportional to varying numbers of active channels).
 20. HeLa cells expressing Cx43-TC were labeled with FLAsH-EDT₂ or ReAsH-EDT₂ as described in (18). The unbound or nonspecifically bound ligand was removed by washing with astringent concentrations of EDT (250 μ M, in HBSS) at the end of the labeling time. Cells were then incubated for 4 to 8 hours in presence of complete medium. The newly synthesized recombinant proteins were stained in a second round of labeling, at the end of the 4 or 8 hour incubation time. The ligand used in the second round was either FLAsH-EDT₂ (for the cells initially labeled with ReAsH-EDT₂) or ReAsH-EDT₂ (for the cells initially labeled with FLAsH-EDT₂). The concentration of each ligand and the staining time were the same as in the first round of labeling. After washing, cells were either fixed in 4% formaldehyde (light microscopy imaging) or were imaged live (using either a BioRad MRC-1024 confocal microscope or a BioRad RTS2000 video rate laser-scanning microscope operating in two-photon mode) in HBSS supplemented with glucose and EDT (10 μ M). The use of a BioRad RTS2000 was particularly useful for recording of time-lapse movies. Because the RTS2000 can acquire optical sections at high frame rates, it is possible to record 3D volumes quickly and follow the labeled proteins in 3D over long periods of time (4D). This multiphoton system was used to record 4D data from the Cx43-TC expressing HeLa cells for up to 6 hours.
 21. J. E. Heuser, T. S. Reese, *J. Cell Biol.* **57**, 315 (1973).
 22. Photoconversion of DAB. After labeling with ReAsH-EDT₂ and live cell imaging, the cells were fixed with 2% glutaraldehyde in sodium cacodylate buffer (0.1 M) (pH 7.4) for 20 min, rinsed in buffer and treated for 5 min in KCN (20 mM), aminotriazole (5 mM), glycine in buffer (50 mM) to reduce nonspecific background. For photoconversion, diamino benzidine (1 mg/ml) in oxygenated sodium cacodylate (0.1 M) was added to the culture dish and the cells were irradiated with 585-nm light from a xenon lamp for 10 to 15 min until a brownish reaction product appeared in place of the red fluorescence. Cells were then washed in buffer and post-fixed in 1% osmium tetroxide for 30 min. Cells were rinsed in distilled water, dehydrated in ethanol, embedded in Durcupan resin, and polymerized at 60°C for 48 hours.
 23. P. A. Takizawa *et al.*, *Cell* **73**, 1079 (1993).
 24. A. R. Maranto, *Science* **217**, 953 (1982).
 25. T. J. Deerinck *et al.*, *J. Cell Biol.* **126**, 901 (1994).
 26. F. Capani *et al.*, *J. Histochem. Cytochem.* **49**, 1351 (2001).
 27. S. Huang, T. J. Deerinck, M. H. Ellisman, D. L. Spector, *J. Cell Biol.* **126**, 877 (1994).
 28. M. E. Martone, T. J. Deerinck, N. Yamada, E. Bushong, M. H. Ellisman, *J. Histochem. Cytochem.* **23**, 261 (2000).
 29. K. Jordan, R. Chodock, A. R. Hand, D. W. Laird, *J. Cell Sci.* **114**, 763 (2001).
 30. A. Terskikh *et al.*, *Science* **290**, 1585 (2000).
 31. J. Lippincott-Schwartz, E. Snapp, A. Kenworthy, *Nature Rev. Mol. Cell Biol.* **2**, 444 (2001).
 32. J. S. Marchant, G. E. Stutzmann, M. A. Leissring, F. M. LaFerla, I. Parker, *Nature Biotechnol.* **19**, 645 (2001).
 33. H. Yokoe, T. Meyer, *Nature Biotechnol.* **14**, 1252 (1996).
 34. U. Lauf, P. Lopez, M. M. Falk, *FEBS Lett.* **498**, 11 (2001).
 35. We wish to thank M. E. Martone for helpful suggestions, discussions, and critical reviewing of the manuscript; K. Jordan for providing pBluescript-Cx43; A. Han for skillful help with the construction of Cx43-TC and its expression in HeLa, NRK cells, and in cardiac myocytes; M. Shah for helpful discussion and for the dye injection experiments and expression in cardiac myocytes; M. M. Falk for helpful discussions and for providing the Cx43-GFP construct used in the electrical coupling experiments; A. Hand for assistance with the immunogold EM. The work described here was conducted at the National Center for Microscopy and Imaging Research at San Diego, which is supported by National Institutes of Health Grant RR04050 awarded to M.H.E. This work is also supported by the Howard Hughes Medical Institute, DOE contract DE-DE-AC03-76SF00098, and NIH grant NS27177 to R.Y.T., NIH grants NS14718 and DC03192 to M.H.E., National Science Foundation MCB-9728338 (to G.E.S.), the Canadian Institutes of Health Research (MT-12241, awarded to D.W.L.). S.R.A. was supported in part by the National Institute of Health grant PO1 DK54441 (awarded to S. S. Taylor).

7 December 2001; accepted 8 March 2002

REPORTS

Ordering in a Fluid Inert Gas Confined by Flat Surfaces

Stephen E. Donnelly,^{1*} Robert C. Birtcher,² Charles W. Allen,² Ian Morrison,¹ Kazuo Furuya,³ Minghui Song,³ Kazutaka Mitsuishi,³ Ulrich Dahmen⁴

High-resolution transmission electron microscopy images of room-temperature fluid xenon in small faceted cavities in aluminum reveal the presence of three well-defined layers within the fluid at each facet. Such interfacial layering of simple liquids has been theoretically predicted, but observational evidence has been ambiguous. Molecular dynamics simulations indicate that the density variation induced by the layering will cause xenon, confined to an approximately cubic cavity of volume ≈ 8 cubic nanometers, to condense into the body-centered cubic phase, differing from the face-centered cubic phase of both bulk solid xenon and solid xenon confined in somewhat larger (≥ 20 cubic nanometer) tetradecahedral cavities in face-centered cubic metals. Layering at the liquid-solid interface plays an important role in determining physical properties as diverse as the rheological behavior of two-dimensionally confined liquids and the dynamics of crystal growth.

Theoretical investigations of the structure of liquids at solid interfaces have indicated that density modulation perpendicular to the interface is likely to occur (1–5). Such layering is expected to occur even in simple hard-

sphere systems and results from the geometrical constraining effect of the solid surface on the atoms or molecules of the liquid, which causes them to order into quasi-discrete layers (6). Recent x-ray scattering ex-

periments on supercooled liquid Ga (7) and an organic liquid (8) have revealed the presence of a small number of distinct layers; however, in the former case dimerization may play a role and in the latter the liquid consists of complex polyatomic molecules, complicating interpretation. We report high-resolution transmission electron microscopy (HRTEM) observations of the interface structure in room-temperature, fluid Xe (critical temperature 16°C) confined in small faceted cavities in electron-transparent Al. Molecular dynamics (MD) simulations provide further insights into the behavior of this simple fluid in small cavities.

HRTEM is a powerful technique for probing the structure of interfaces such as grain boundaries and free surfaces in solids but is generally not suitable for studying the structure of interfaces involving liquids. In addi-

¹Joule Physics Laboratory, Institute for Materials Research, University of Salford, Manchester M5 4WT, UK. ²Materials Science Division, Argonne National Laboratory, Argonne IL 60439, USA. ³National Institute for Materials Science, 3-13 Sakura, Tsukuba 305, Japan. ⁴National Center for Electron Microscopy, LBNL, Berkeley, CA 94720, USA.

*To whom correspondence should be addressed. E-mail: s.e.donnelly@salford.ac.uk

REPORTS

tion to the x-ray scattering work mentioned above, HRTEM studies on the interface of crystalline Pd₃Si and amorphous Pd₈₀Si₂₀ (9) have also revealed the presence of layers at the interface in the amorphous phase; however, in this study, there was no certainty that the structure near the interface in the amorphous solid reflects that at a liquid-solid interface.

Here, we take advantage of the tendency of inert gases, when energetically injected into metals, to cluster together with lattice vacancies to form small bubbles with radii of a few nanometers. A spherical bubble at thermal equilibrium will be under a pressure given by $P = 2\gamma/R$, where γ is the interface free energy and R is the radius of the bubble (10). For inert gas bubbles with radii on the order of a few nanometers, this yields giga-

pascal pressures. Room-temperature bubbles in which the inert gases Ar, Kr, and Xe were under sufficiently high pressures to be in the solid phase have been identified by electron diffraction (11, 12) and lattice imaging (13). The small inert gas-filled cavity in a thin metal film is a useful high-pressure cell, permitting transmission electron microscopy (TEM) studies.

Specimens suitable for TEM were prepared by electrochemical jet thinning to perforation of well-annealed, high-purity Al discs. Thinned specimens were implanted with 30-keV Xe⁺ ions to a total dose of 2×10^{19} ions m⁻², yielding Xe bubbles with diameters of up to 15 nm that contained Xe in either the solid or the fluid state. HRTEM was carried out with the 1-MeV electron microscope (JEM-ARM 1000, JEOL) at the National Institute for Materials Science (formerly the National Research Institute for Metals) in Tsukuba, Japan. An off-axis im-

aging technique was used in which a few degrees of tilt away from the Al <110> zone axis and non-Scherzer defocus are employed to reduce the image contrast from low-index Al reflections (14). This results in high-resolution images which, at specific values of defocus, contain little contrast from the Al matrix, whereas contrast is clearly visible both from solid Xe in some cavities and in the form of fringes at the facets of cavities containing fluid Xe. Cavities are generally observed to be tetradecahedral in shape—that is, {111} octahedra with 6 {100} truncations (14). Images were recorded on photographic negatives at a magnification of 800,000× and were digitized (at 1200 pixels per inch) with contrast reversal to yield positive images. The contrast was optimized and, for specific values of defocus, no additional image processing or filtering was carried out. An example of such an image is presented in Fig. 1. Through-focus sequences of images were re-

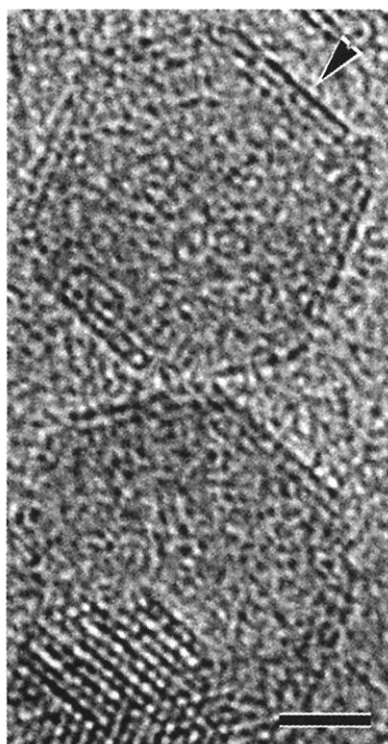


Fig. 1. High-resolution TEM image of faceted, Xe-containing cavities in Al at room temperature. The Xe in the two large cavities is fluid; in the small cavity at the bottom of the figure, whose image overlaps one of the large cavities, Xe is solid. Note that, although their images slightly overlap, the two large cavities are not in contact. Image overlap results from the distribution of cavities through the depth of the Al foil. [When contact between cavities occurs, immediate coalescence is observed (18).] The image was recorded in a 1-MeV JEOL ARM-1000 microscope at an objective lens defocus of +72 nm. The contrast transfer function of the microscope under these conditions, combined with a small degree of tilt, results in very little intensity from the Al lattice in the micrograph (14), enabling layering in the fluid Xe to be clearly seen. The arrow shows the facet from which the data presented in Fig. 2A have been obtained. Bar, 2.5 nm.

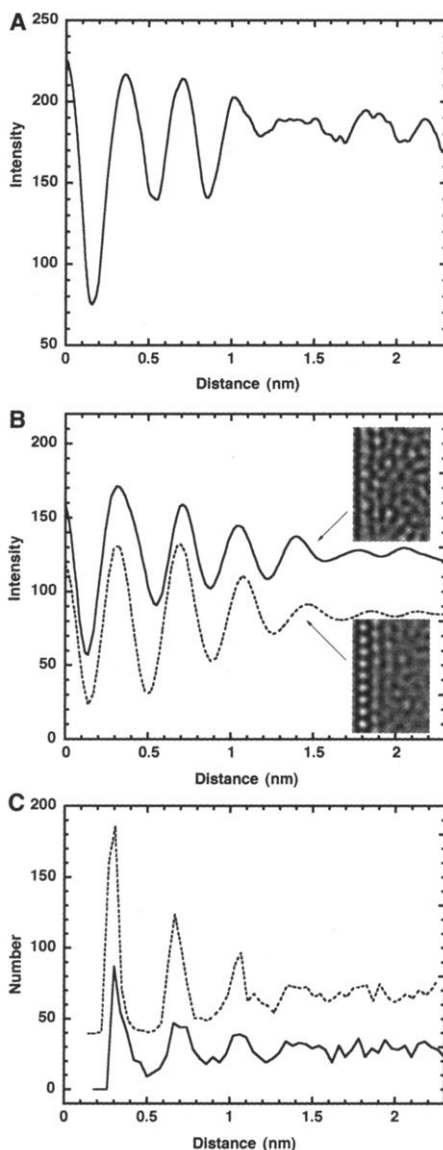


Fig. 2. Observed and simulated intensity variation in HRTEM images due to layering in the fluid Xe. (A) Variation in intensity as a function of distance within the cavity measured in a direction normal to the facet indicated by the arrow in Fig. 1. The figure shows the presence of three fringes. (B) Intensity variation in two simulated HRTEM images of an interface between fluid Xe and solid Al at an objective lens defocus of +72 nm. Input for the image simulation was obtained from MD simulations with "corrugated" (dashed curve) and "flat" (solid curve) potentials respectively (20). (For clarity, the origin of the lower curve has been displaced by 20 units downwards.) The inset images are the areas of the simulated images from which the intensity variation has been taken. The width of the inset image corresponds, in each case, to 2.3 nm. The height of the image is the approximate distance over which the intensity variation normal to the interface has been summed. (C) Number of Xe atom centers in 0.04-nm slices parallel to the Xe/Al interface in the MD simulations as determined with "corrugated" (dashed curve) and "flat" (solid curve) potentials, respectively. The presence of three distinct layers is clearly indicated in each case. (For clarity, the origin of the upper curve has been displaced by 40 units upwards.) The exact density of the Xe in the cavities is not known. For this reason and because of the approximate nature of the Xe-Al potential, we attach no importance to the differences in the fringe spacings between the observed and simulated images or between those in the two simulated images.

corded, and these were Fourier filtered with an annular filter to remove contrast from the Al lattice, before being compared with images simulated with the MacTempas multislice program (15) incorporating the relevant parameters for the JEOL ARM-1000 microscope (16).

Observations were made at room temperature on Al containing Xe precipitates. The HRTEM image in Fig. 1 shows two large faceted cavities containing fluid Xe. The cavities are seen in $\langle 110 \rangle$ projection with Al $\{111\}$ and $\{100\}$ planes approximately normal to the plane of the image. A smaller cavity containing solid Xe can also be seen in the bottom left-hand corner of this figure. Fringes are visible in the Xe at all or most facets of more than 100 cavities containing fluid Xe that have been recorded on film and videotape. The fringes result from variation of contrast normal to the facets as illustrated in Fig. 2A for a $\{111\}$ facet (marked with an arrowhead) of the cavity at the top of Fig. 1. This is typical of the contrast associated with most facets in most cavities containing fluid Xe.

To interpret this intensity variation, atomic configurations resulting from MD simulations of a slab of fluid Xe (modeled as a dense Lennard-Jones fluid) in contact with a planar solid interface were used as input to multislice image simulations (15). Solid Xe in cavities in Al has been observed to have a lattice parameter about 1.5 times that of the Al matrix (17, 18). Melting of solid Xe has been observed to be associated with a cavity volume change of $\sim 30\%$ (19). To obtain the atomic configuration of fluid Xe, the MD simulations involved the expansion of solid Xe (with a lattice constant 1.5 times that of the Al) by 30%, resulting in the melting of the Xe. Two simulations were performed, one in which the equipotential surfaces near the interface were corrugated, resulting in ordering in the first layer that was not discernible in

the experimental images. The second simulation used a planar potential, resulting in flat equipotential surfaces (20). In both cases the simulated images yield contrast that also varies normal to the $\{111\}$ interface as shown in Fig. 2B. The insets in Fig. 2B are the simulated images from which the contrast variations are derived.

In both experiment and simulations, three clear fringes are observed. The origin of the fringes in the simulated images is the layering of Xe atoms in the fluid at the interface. This layering can be clearly seen in Fig. 2C, where the number of Xe atoms in the MD calculations in thin slices parallel to the interface is plotted as a function of distance. Inspection of Fig. 2, B and C, reveals that (at a defocus of +72 nm) the positions of the maxima in electron intensity in the image (bright fringes) correspond to the positions of the maxima in the Xe density. This indicates that the contrast variations in the experimental image (Fig. 1) also result from three distinct layers of Xe at the interface. The results provide conclusive evidence for layering at a fluid/solid interface in a simple fluid.

Solid Xe in tetradecahedral cavities in face-centered cubic (fcc) metals has a fcc structure; however, the presence of three distinct layers extending about 1 nm into the fluid from each facet of the cavity raises the question of the atomic configuration likely to result in Xe in a cavity whose dimensions are on the order of 2 nm, that is, in which the layers occupy the full width of the cavity in all directions. To avoid possible ordering arising from unrealistic corrugations in the potential due to the atoms making up the facets of the cavity, the planar repulsive potential (20) was used in a simulation in which Xe was confined in an approximately cubic cavity. The starting point for the simulation was room-temperature, solid fcc Xe with a lattice constant of 0.61 nm within an approx-

imately cubic cavity. The facets of the structure were $\{111\}$, $\{110\}$, and $\{112\}$ fcc planes as in the previous simulation. However, in this case, the cell contained only 180 Xe atoms. The cell was expanded by 30% (in volume) and heated to 2000 K for 1 ps to randomize the atomic positions of the Xe atoms. The cell was then quenched back to room temperature and the volume of the cell incrementally decreased (a 10-ps simulation was performed between each volume increment) and the fluid structure monitored as the density increased.

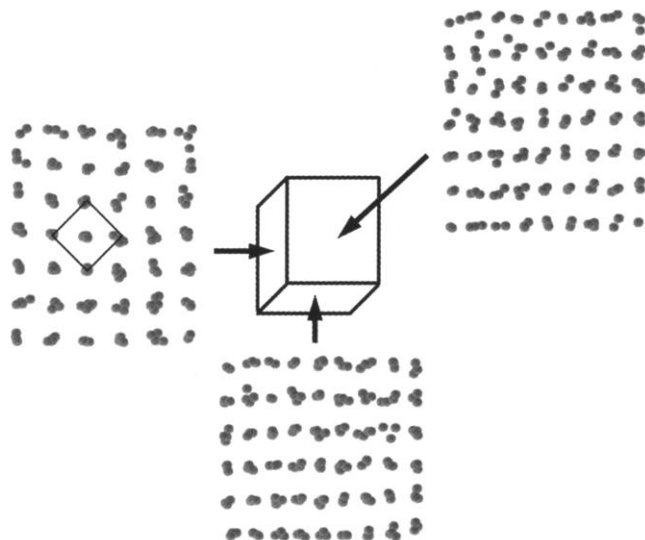
The simulation revealed that interface ordering can lead to what appears to be three-dimensional (3D) ordering. At densities below 1.60×10^{22} atoms cm^{-3} , layering in the Xe similar to that shown in Fig. 2C and extending across the cavity width was observed perpendicular to all facets. Although the density maxima thus lay approximately on a 3D lattice, a high degree of disorder was present, and trajectories of individual Xe atoms revealed that the Xe still exhibited fluid behavior. The density fluctuations arose from longer residence times of atoms in the vicinity of the lattice points. On compression to the density of solid Xe at room temperature (1.7×10^{22} atoms cm^{-3}), the Xe atoms occupied positions close to lattice points defined by the intersection of orthogonal layers. However, instead of the fcc structure observed in bulk material, the Xe clearly condensed into a body-centered cubic (bcc) phase (Fig. 3). This is an example of the structure of the crystal being controlled by its geometry, as has been observed in recent theoretical analyses of atoms and molecules confined to small dimensions both two dimensionally (6, 21) and three-dimensionally (22). It should be noted that in a fcc arrangement in this cell, 51% of the 180 atoms in the layers would be in contact with the cavity facets compared with 61% in the case of the observed bcc configuration.

Our results indicate the possibility of nucleating, in cavities in selected materials, clusters of inert gases, and indeed other elements, with crystallographic structures determined by the geometry of the cavities (23). Such structures would not occur in unconfined systems, and the nanoclusters may exhibit unusual electronic, optical, and other properties.

References and Notes

1. A. Bonissent, B. Mutaftschiev, *Philos. Mag.* **35**, 67 (1977).
2. J. W. Cahn, R. Kikuchi, *Phys. Rev. B* **31**, 4300 (1985).
3. B. B. Laird, D. J. Haymet, *Chem. Rev.* **92**, 1819 (1992).
4. F. Spaepen, *Solid State Phys.* **47**, 1 (1994).
5. M. Plischke, D. Henderson, *J. Chem. Phys.* **84**, 2846 (1986).
6. J. N. Israelachvili, *Intermolecular Forces and Surface Forces* (Academic Press, San Diego, CA, 1992), pp. 261-275.
7. W. J. Huisman *et al.*, *Nature* **390**, 379 (1997).

Fig. 3. The structure resulting from a MD simulation of dense fluid Xe in a tetragonal cavity measuring 2.06 nm by 2.26 nm by 1.88 nm. See text for details. The three projections are along directions normal to the cavity surfaces, as indicated by the arrows. The Xe atoms lie close to a bcc lattice that presents four $\{110\}$ planes and two $\{100\}$ planes to the surfaces of the cavity. The body centered unit cell (rotated by 45° with respect to the cavity axes) is indicated by the square. The Xe density is $1.64 \pm 0.1 \times 10^{22}$ atoms cm^{-3} (27).



8. C.-J. Yu, G. Richter, A. Datta, M. K. Durbin, P. Dutta, *Phys. Rev. Lett.* **82**, 2326 (1999).
 9. J. M. Howe, *Philos. Mag.* **A 74**, 761 (1996).
 10. S. E. Donnelly, *Radiat. Effects* **90**, 47 (1985).
 11. C. Templier, R. J. Gaboriaud, H. Garem, *Mater. Sci. Eng.* **69**, 63 (1984).
 12. A. Vom Felde *et al.*, *Phys. Rev. Lett.* **53**, 922 (1984).
 13. S. E. Donnelly, C. J. Rossouw, *Science* **230**, 1272 (1985).
 14. K. Furuya, N. Ishikawa, C. W. Allen, *J. Microsc.* **194**, 152 (1999).
 15. MacTempas; Total Resolution, Berkeley, CA.
 16. Experimental and simulated through-focus sequences are available on Science Online at www.sciencemag.org/cgi/content/full/1068521/DC1.
 17. S. E. Donnelly, K. Furuya, M. Song, R. C. Birtcher, C. W. Allen, *Proceedings of the International Centennial Symposium on the Electron*, A. Kirkland, P. D. Brown, Eds. (Institute of Materials, London, 1999), pp. 306–312.
 18. R. C. Birtcher *et al.*, *Phys. Rev. Lett.* **83**, 1617 (1999).
 19. S. E. Donnelly *et al.*, unpublished data.
 20. The starting point for the fluid Xe simulations was a tetragonal slab of solid, fcc Xe with a lattice parameter 1.5 times that of Al confined between two walls, 8.06 nm apart, each consisting, in the first instance, of three {111} Al planes. The dimensions of the cell were 8.06 nm, 6.86 nm, and 7.43 nm in the [1,1,1], [1,–1,0], and [1,1,–2] directions, respectively, and the crystallographic axes of the Xe were aligned with those of the Al. Periodic boundary conditions were used in the two latter directions. A total of 6720 Xe atoms were used in the simulations. To achieve fluid Xe, the volume of the cell was expanded by 30%, and the temperature was increased to 2000 K for 1 ps, resulting in complete disordering of the Xe layer. The system was then cooled back to 300 K and the simulation continued for a further 10 ps. Two separate simulations were performed: in the first, which was performed with the MOLLY code (24), a Lennard-Jones interaction potential was used for all interactions, including the Xe-Al interaction. With this approach, however, equipotential surfaces near the interface were corrugated due to the individual atoms in the interface. This gave rise to a keying effect that resulted in ordering in the first Xe layer that was visible in the simulated images; however, such ordering was not observed in the experimental images. The second approach was to replace the three Al layers by a planar repulsive potential of the form $V(R) = c/R^{12}$, where R is the distance from the facet and c was chosen to give equivalence to the repulsive term in the Lennard-Jones potential. This simulation was performed with the DLPOLY code (25) with an adaptation of the external field routine to represent the planar confining potential. This gave rise to equipotential surfaces that were flat. A realistic Xe-Al potential, which is not currently available, would result in equipotential surfaces between these two extremes. The planar potential was also used for all six facets in the simulation of the small cubic cavity. Although both simulations are physically unrealistic as far as the Xe-Al interaction is concerned, in addition to inducing ordering in the first Xe layer, the effect of changing the Al-Xe potential is to change the separation between the Xe and Al interface layers. Hence in this work, the separation between the first Xe layer and the Al layers has no quantitative importance.
 21. M. Schmidt, H. Löwen, *Phys. Rev. E* **55**, 7228 (1997).
 22. W. K. Kegel, H. Reiss, H. N. W. Lekkerkerker, *Phys. Rev. Lett.* **83**, 5298 (1999).
 23. Although metastable Cu precipitates with a bcc structure have been identified in irradiated Fe alloys, it is likely that factors other than the confining geometry may play a role in this system (26).
 24. K. Refson, *Comput. Phys. Commun.* **126**, 310 (2000).
 25. W. Smith, T. R. Forester, *J. Mol. Graphics* **14**, 136 (1996).
 26. S. Pizzini, K. J. Roberts, W. J. Pythian, C. A. English, G. N. Greaves, *Philos. Mag. Lett.* **61**, 223 (1990).
 27. Density is determined from the number of atoms contained in a tetragonal box whose faces are located

half way between the surface layers and the second layer in each direction. This avoids problems associated with defining the volume associated with the surface atoms.

28. S.E.D., R.C.B., C.W.A., and U.D. acknowledge funding from the National Institute for Materials Science, for collaborative visits to Japan; S.E.D. acknowledges

funding from the Materials Science Division at Argonne National Laboratory for extended visits to the laboratory.

29 November 2001; accepted 12 March 2002
 Published online 21 March 2002;
 10.1126/science.1068521

Include this information when citing this paper.

External Reflection from Omnidirectional Dielectric Mirror Fibers

Shandon D. Hart,¹ Garry R. Maskaly,¹ Burak Temelkuran,^{1,3}
 Peter H. Prideaux,³ John D. Joannopoulos,^{2,3} Yoel Fink^{1,3*}

We report the design and fabrication of a multilayered macroscopic fiber preform and the subsequent drawing and optical characterization of extended lengths of omnidirectional dielectric mirror fibers with submicrometer layer thickness. A pair of glassy materials with substantially different indices of refraction, but with similar thermomechanical properties, was used to construct 21 layers of alternating refractive index surrounding a tough polymer core. Large directional photonic band gaps and high reflection efficiencies comparable to those of the best metallic reflectors were obtained. Potential applications of these fibers include woven fabrics for radiation barriers, spectral authentication of cloth, and filters for telecommunications.

Polymer fibers are ubiquitous in applications such as textile fabrics because of their excellent mechanical properties and the availability of low-cost, high-volume processing techniques; however, control over their optical properties has so far remained relatively limited. Conversely, dielectric mirrors are used to precisely control and manipulate light in high-performance optical applications, but the fabrication of these typically fragile mirrors has been mostly restricted to planar geometries and remains costly. We combined some of the advantages of each of these seemingly dissimilar products in the fabrication of polymeric fibers with an exterior multilayer dielectric mirror. Thermal processing techniques were used to reduce a macroscopic layered dielectric structure to submicrometer length scales, creating a fiber having a photonic band gap in the mid-infrared (mid-IR). Where previous experimental and theoretical work on multilayer fibers has focused on the purpose of light transmission through a hollow core (1–3), we used multiple dielectric layers on the exterior of a mirror fiber to create the potential for new conformal reflector functionality (4). These fibers could be incorporated into woven fabrics for precise spectral identity verification, such as a unique optical bar code; they could also be used as

flexible radiation barriers or as filters in telecommunications.

A typical dielectric mirror (also called a one-dimensional photonic crystal) is a planar stack of dielectric layers made of two alternating materials with different refractive indices. Although these mirrors do not possess a complete photonic band gap, it has been shown that they can be designed to efficiently reflect light of all incident angles and polarizations across broad, selectable frequency ranges (5, 6). This advance has inspired interest in the use of omnidirectional dielectric mirrors in applications requiring optimal confinement or reflection of light at all external angles, such as optical cavities or hollow waveguides. The theory and properties of planar multilayer dielectric mirrors and omnidirectional reflectors have been explored elsewhere (5–10).

The degree of use of all types of dielectric mirrors has been impeded by the cost and complexity associated with their fabrication and by the difficulties associated with depositing these mirrors on nonplanar surfaces. Weber and co-workers (11) reported the fabrication of free-standing, graded-thickness polymeric dielectric mirrors with relatively low-refractive-index contrast between adjacent birefringent layers. The system employed in our work uses amorphous materials having high-refractive-index contrast. This has some advantages over a low-contrast structure in that the evanescent decay lengths and electric field power densities of reflected electromagnetic (EM) waves are much smaller in the mirror stack, making it

¹Department of Materials Science and Engineering,

²Department of Physics, ³Research Laboratory of Electronics, Massachusetts Institute of Technology, Cambridge, MA 02139, USA.

*To whom correspondence should be addressed.